Plasmonic Imaging of Oxidation and Reduction of Single Gold Nanoparticles and Their Surface Structural Dynamics

Adaly Garcia,[†] Shaopeng Wang,[‡] Nongjian Tao,[‡] Xiaonan Shan,[*,§] Yixian Wang[*,†]

[†] Department of Chemistry and Biochemistry, California State University, Los Angeles, 5151 State University Dr, Los Angeles, CA 90032

[‡] Center for Biosensors and Bioelectronics, Biodesign Institute, Arizona State University, 1001 S McAllister Ave, Tempe, AZ 85281

[§] Department of Electrical & Computer Engineering, University of Houston, 4800 Calhoun Rd, Houston, TX 77004

Supporting Information Placeholder

ABSTRACT: Gold nanoparticles (AuNPs) have been widely used in catalytic electrochemistry. Heterogeneity in size, shape, and surface sites leads to variable, particle-specific catalytic activities. Conventional electrochemical methods can only obtain the collective responses from all the catalytic nanoparticles on the electrode surface; the heterogeneity of particle performance will be averaged. Alternatively, plasmonic electrochemical imaging (PECi) is capable of imaging the electrochemical activities at individual nanoparticles. In this work, PECi was used to image the oxidation and reduction of the gold surface at individual AuNPs, and their associated structural alterations were successfully measured. We have studied the electrochemical responses from gold nanocubes, gold nanorods, and gold nanowires with PECi and observed different surface redox activities. We have also demonstrated the capability of monitoring the surface dynamics at individual AuNPs utilizing characteristic PECi derived cyclic voltammograms (CVs).

KEYWORDS: *Gold nanoparticles, plasmonic electrochemical imaging, surface facets, single nanoparticle electrochemistry, nanocubes, nanowires, nanorods.*

Since Faraday reported the first observation of gold nanoparticles (AuNPs) in 1857, they have been extensively used in catalytic electrochemistry and energy research.[1–3] The catalytic properties of AuNPs are primarily dependent on their surface structure since different facets provide different active sites, which has been demonstrated by single-crystal electrodes.[4–6] Determining the surface structure of AuNPs and monitoring the structural alteration during the reactions is thus essential to understand their relationship with the catalytic efficiency and help with designing new catalysts. Electrochemical (EC) methods, such as cyclic voltammetry (CV), could provide important surface structure information. For example, the surface of the gold film and AuNPs will be oxidized and reduced when the potential is applied through the potentiostat (Scheme 1). The variations in energy states due to different surface structure will generate characteristic cyclic voltammograms (CVs). Previous studies using single-crystal Au electrodes with different facets (i.e. (100), (110), (111)) have shown that each facet has its "fingerprints" in the form of unique minor peaks in the CVs.[4,7] A similar approach can be applied to AuNPs by depositing them onto an inert electrode surface (e.g., glassy carbon electrode) and carrying out the EC test. As a result, averaged information of all AuNPs in the sample can be provided.[8–11] However, heterogeneity is a general feature for AuNPs, which can only be revealed by investigating individual AuNPs. Plasmonic electrochemical imaging (PECi), a surface plasmon resonance (SPR) based imaging technique, has been used to study surface electrochemistry at individual NPs.[12–14] A typical experimental setup of using PECi for quantifying the oxidation and reduction of the oxidation/reduction of the surface of a AuNP is shown in Scheme 1.

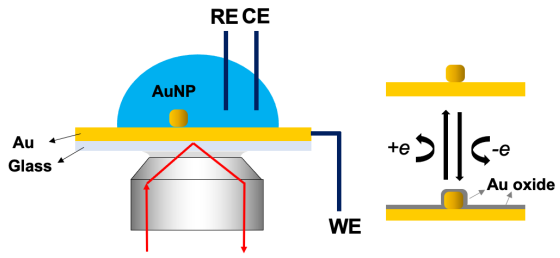

Scheme 1. Schematic of the PECi experimental setup and the oxidation/reduction of the surface of a AuNP.

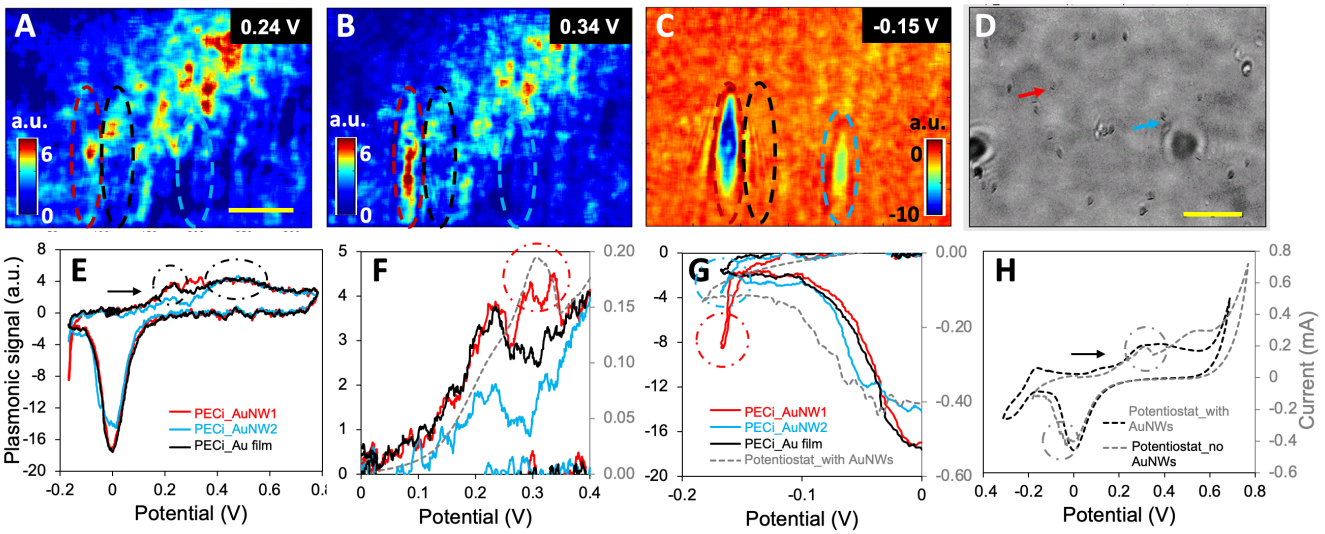

Figure 1. Representative PECi images and CVs from AuNWs. (A-C) PECi images of a AuNWs-coated Au film at different voltages as labeled in the figures. (D) Transmitted optical image of the same area with A-C. Pixel size is approximately 82 nm. (E) PECi CVs (plotting of averaged signals within selected areas from PECi images versus scanning voltage) of two AuNWs (red and blue solid lines, extracted from the two tail areas in A-C marked by red and blue dashed circles, corresponding to the two AuNWs marked by arrows in D) and background Au area (black solid line, extracted from the black dashed circled area in A-C). (F, G) The zoom-in of (F) oxidation peaks and (G) reduction peaks and overlapping with the potentiostat CV from H (grey dashed line); (H) Potentiostat CVs of the whole electrode before (black dashed line) and after depositing AuNWs (grey dashed line). Scale bar: 5 μm. Scanning rate: 0.2 V/s. Black arrows in E and H represent the direction of forward scan.

Herein we demonstrate the use of PECi to monitor the oxidation and reduction of the surface of individual Au NPs and to reveal information of the surface structure dynamics. Commercially available AuNPs, either nanocubes (NCs), nanorods (NRs), or nanowires (NWs), were directly deposited on a gold film, which works as both the SPR sensing chip and the working electrode for the three-electrode EC cell. The reference electrode and counter electrode were a chloridized Ag wire quasi-reference electrode and a Pt coil, respectively. The EC cell was mounted on a high numerical aperture oil immersion objective with refractive index matching oil. P-polarized light was directed onto the gold film through the objective for plasmonic excitation, and the reflected light was collected with the same objective and captured by a CCD camera for imaging.[13] Electrochemical reactions on the AuNPs were controlled by directly applying a potential onto the gold film. Each NP's SPR image has a parabolic tail originating from the scattering of the plasmonic wave by the NP.[15] The observed signal of each NP is the summation of the partially reflected light and scattered plasmonic wave associated with the optical properties (e.g., permittivity) of the NP.[12,13] Electrochemical reaction will oxidize the AuNPs and induce the corresponded changes in the optical properties of the NPs. The optical responses are proportional to the amount of the electrochemical reaction on the particle surface per unit time (reaction rate). Thus, by extracting the time-dependent SPR intensity changes within the parabolic tail area, a PECi CV can be plotted for each NP. To directly compare the AuNPs and Au substrate activities, we chose not to block the gold film with cytop[13] and deposited AuNPs directly. The locations of the AuNPs can be identified by their distinct parabolic tails and their characteristic EC activities associated with the surface facets. The Au substrate is a thin film deposited by electron beam evaporation, which is reported to be dominated with (111) facet.[16] On the other hand, the AuNCs, AuNRs, and AuNWs are dominated with (100) and/or (110) facets[8,10,17,18]. The EC "fingerprints" for these different facets include a couple of anodic peaks originating from the first electron transfer during gold surface oxidation. Different facets will generate different numbers of peaks: three for (100) facet, two for (110) facet, and one for (111) facet, due to the different energy states of the surface.[4,7] Moreover, both (100) and (110) facets generate an additional cathodic peak during the reduction process, with the peak from (100) being more negative than that from (110).[4,7] In contrast, (111) facet has only one oxidation peak and no additional cathodic peaks.[4,7]

Figure 1 shows several snapshots of the PECi images of multiple AuNWs (75 nm in diameter, 1 μm in length) at different potentials. The image contrast represents the intensity of the derivative of original SPR signals over time at all pixels. At 0.24 V, no contrast of the AuNWs was observed because of oxidation at both bare Au and AuNWs areas (Fig. 1A). The signal is not uniformly

distributed due to the air bubble present in the immersing oil. The PECi image at 0.34 V shows the distinct response from a single AuNW (Fig. 1B, circled by red dashed line). After the Au reduction (for example, at -0.02V), the gold oxide layer on both AuNWs and gold film were reduced simultaneously, which lead to the diminished contrast on the PECi image (Fig.S1A). When the potential was scanned to -0.15 V, a significant cationic signal was produced by the two AuNWs (red dashed circled area and blue dashed circled area in Figs.1A-C) while no reaction occurred in the background. This additional anodic peak's potential agrees with the result produced by (100) single crystal electrode.[4]

The plasmonic signal of the AuNW tail area was plotted versus the applied potential to form the voltammetry of the AuNW. It was compared with the signal from adjacent bare Au film area (black dashed circled area in Fig.1A-C). We can see the obvious differences between the two areas. Note that although the signal within the AuNW tail area is a combination of the signals from both the AuNW and the underlying Au film, the contribution from AuNW dominates. Both the AuNW and Au film areas produce a similar oxidation peak at around 0.23 V and a broad oxidation peak ranging from 0.3 V to 0.6 V (marked by black dash dotted circles in Fig.1E). These peaks come from the (111) facet of the gold film. Interestingly, the AuNW tail area produced two additional peaks at potential starting from 0.28 V to 0.36 V (marked by red dash dotted circle in Fig.1F). These peaks correspond to the oxidation peaks from (100) facet reported from the single crystal planar electrodes.[4,7] This observation has demonstrated the unique capability of PECi to image the structural dynamics of single nanoparticles. A significant cathodic current around -0.17 V (red dash dotted circle in Fig. 1G and blue particles in Fig. S2A) further supported our observation. The second AuNW, located in the blue dashed circle in Figs. 1A-C, also showed a reduction current at the characteristic potential around -0.17 V (blue dash dotted circle in Fig. 1G)., although the (100) oxidation "fingerprints" is relatively weak. This is due to the relatively strong background oxidation. The observation of (100) facets at AuNWs is in accordance with the fact that twinned pentagonal nanowires (confirmed by the manufacturer) consist of elongated (100) facets.[17,19,20] CVs from the electrochemical recording were shown in Fig. 1H to compare the overall electrode performance before and after adding AuNWs. It is very obvious that more minor peaks appeared after the addition of the nanoparticles (marked by grey dash dotted circle in Fig.1H).

Note that there is oxygen evolution reaction (OER) related current at ~0.7V in the potentiostat CVs (Fig. 1H). Plasmonic image is capable to measure and image the OER reaction. However, in this paper we are focusing on imaging the oxidation and reduction of the Au nanoparticles, and we have modified the optical signal process algorithm to amplify the Au oxidation responses and minimize the OER reaction responses. Instead of using the de-convolution formula,[21] the derivative of intensity was used to minimize the signal from the oxygen evolution reaction and accurately extract the localized oxidation and re-duction current.

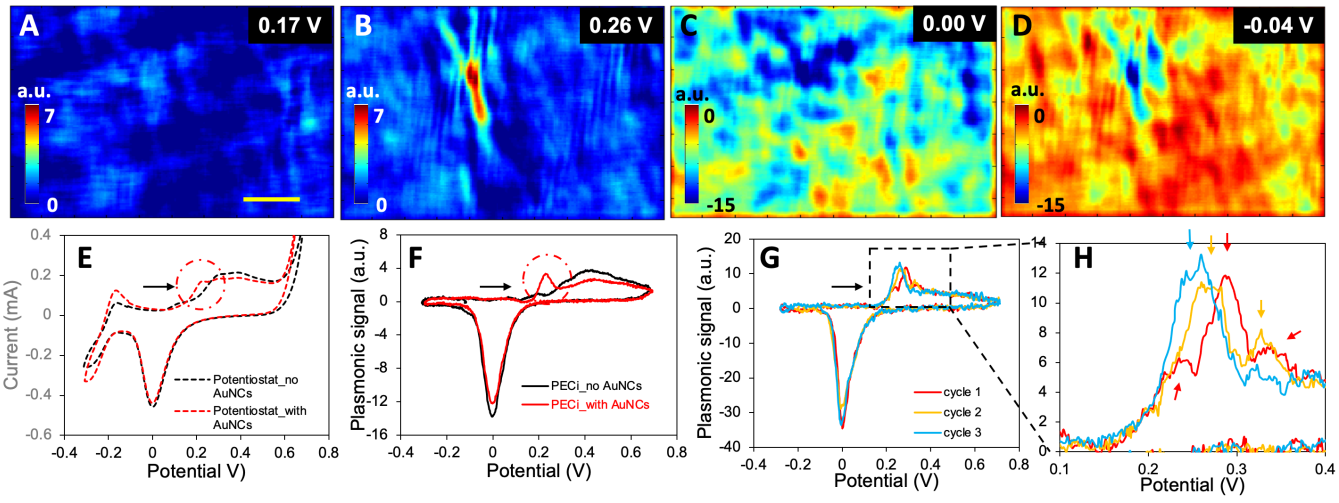

Figure 2. Representative PECi images and CVs from AuNCs. (A-D) PECi images of a AuNCs-coated Au film at different voltages as labeled in the figures. Pixel size is approximately 123 nm. (E) Potentiostat CVs before (black) and after (red) depositing AuNCs. (F) PECi CVs of the whole sensing area before (black) and after (red) depositing AuNCs. (G) Multiple cycles from a PECi CV extracted from the AuNC area from B and (H) zoom-ins of the oxidation and reduction peaks as labeled in G. Scale bar: 5 μm. Scanning rate: 0.2 V/s. PECi images were extracted from the second cycle. Black arrows in E-G represent the direction of forward scan.

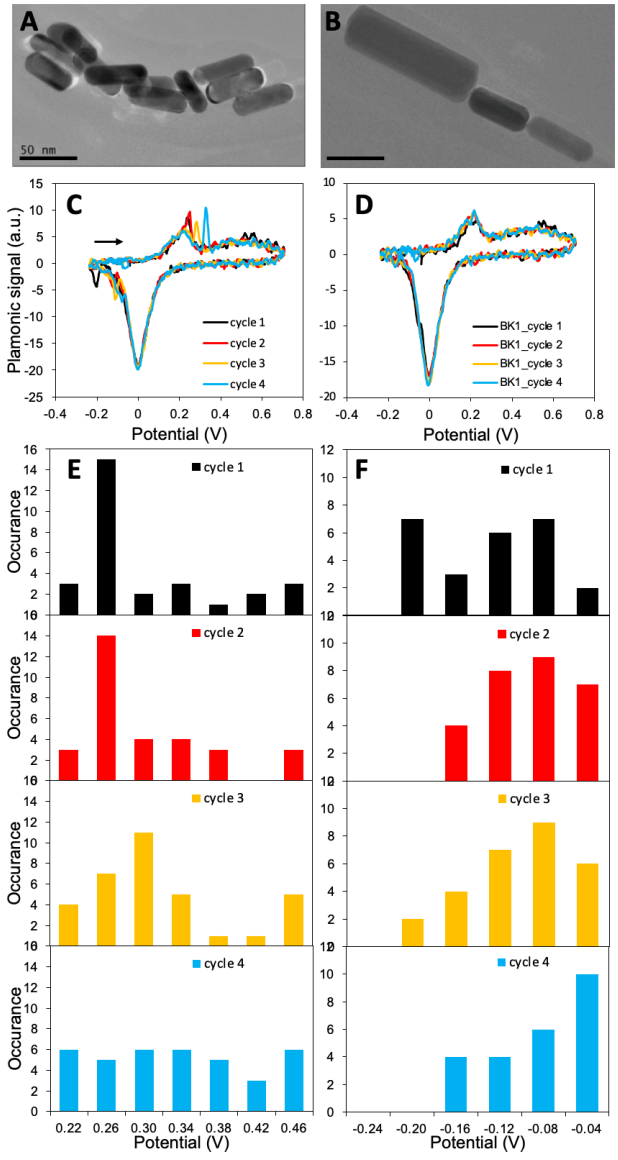

Figure 3. Representative TEM and PECi images and CVs from AuNRs. (A, B) TEM images of a group of AuNRs from the same batch. (C, D) PECi CVs of a AuNR (C) and its adjacent Au area (D). (E, F) Histograms of the distribution of minor oxidation (E) and reduction peaks (F) from individual scanning cycles indicated by different colors. Scanning rate: 0.2 V/s. The black arrow in C represents the direction of forward scan.

We have also studied the oxidation and reduction process of AuNCs (60 nm in size) on Au substrate with PECi. Figs. 2A-D show several snapshots of the PECi images of the sample at different potentials. The significant response contrast in Fig.2B is caused by the oxidation of the AuNCs, which is at a different potential compared to the underlying gold film. This is also demonstrated by both potentiostat (Fig.2E), and PECi CVs (Fig.2F) averaged from the whole sensing area, in which a new anodic peak appeared around 0.26 V after depositing AuNCs (marked by the red dash dotted circles in Fig.2E and F). Figs.2C and D show the oxide reduction process on the gold substrate and the AuNCs, respectively. We have also shown in Fig.S2B that the AuNCs tail area generated anodic minor peaks around similar potential range. PECi CVs extracted from the AuNC area allow us to study the particle structure dynamics during multiple CV scans. As shown in Fig. 2G, three cycles were recorded, and the corresponding PECi responses from the AuNCs area were plotted. Interestingly, the peak distribution varies among the three scans. Specifically, the number of minor anodic peaks between 0.2 and 0.4 V (Fig. 2H) decreases from three (red arrows, cycle 1) to two (orange arrows, cycle 2), and to one (blue arrow, cycle 3) eventually. This could be caused by the structural transformation from the cubic structure ((100) dominated) to the spherical structure (polycrystalline).

The facets of gold nanorods can be dominated by (100) and/or (110) dependent on the growth condition. An idealized pentagonally twinned rod is expected to have five (100) side faces, while in reality, the side faces of the nanorods could be not well-developed and are therefore rounded and consist both (100) and (110).[19] To demonstrate the PECi's capability, we have studied the redox reactions of gold nanorods (AuNRs) (40 nm in diameter, 180 nm in length). A TEM survey of the AuNRs used in the studies indeed demonstrates the variety of AuNRs from the same batch, as shown in Figs. 3A and 3B. The AuNRs in Fig. 3A are smaller and rounded on the side, while the one large AuNR in Fig. 3B shows defined side faces. These AuNRs consist of different combinations of facets, which can be analyzed using the PECi approach. Two representative sets of PECi CVs of AuNRs are shown Fig. 3C and Fig.S2C. Characteristic minor redox peaks appeared in both reduction and oxidation regions from the AuNR (Fig. 3C), while the adjacent bare gold area shows typical (111) properties (Fig. 3D). Moreover, the minor peaks shift during the multiple scans at the AuNR area, while the signal remains consistent for all cycles at the bare gold area. We further analyzed the distribution of the minor redox peak potentials from 16 AuNRs, as shown in Figs. 3E and 3F. The PECi CVs for the other 15 AuNRs are shown in Fig. S3. The total occurrence from each cycle is higher than 16 due to the existence of multiple minor peaks within one cycle. During the first cycle, there was a high occurrence of cathodic peaks (Fig.3F) between -0.24 V to -0.20 V, which is about 0.2 V more negative than the major cathodic peak. This minor cathodic peak position is the "fingerprint" of (100) facets [4,7]. There are also plenty of minor peaks closer to the major cathodic peak (-0.08 V to -0.16 V, which fit the "fingerprint" of (110) facets[4,7]. This demonstrates the co-existence of (100) dominated and (110) dominated facets on AuNRs, as suggested by the literature[19] and TEM results. Analysis from both reduction and oxidation peaks indicates an overall positive shift of the minor peak potentials. Statistically, taking the anodic peaks for an example (Fig.3E),

higher occurrence of peaks around 0.22V to 0.26 V was observed at cycles 1 and 2, compared to cycles 3 and 4, which is likely due to more presences of (100) facets on the original AuNRs during the early scans. The occurrence decreased during the oxidation and reduction scans, which suggests a gradual surface structural reconstruction that involves conversion of (100) facets to (110) and/or (111) facets happens. Cathodic peak distribution also agrees with the observation given that the highest abundant peaks moved to less negative positions from cycle 1 to later cycles.

In conclusion, we have successfully used PECi to image the surface redox reaction at single AuNPs and compared their activities and the associated surface structure with gold film. We were able to identify (100) and (110) facets from different AuNPs utilizing their distinct minor peaks as reported for single crystal electrodes. Slight differences exist among NPs as they varied in size and shape. Surface structure alteration was also observed. Future aims will be combining PECi with high-resolution structural imaging tools, such as scanning tunneling microscopy, to fully understand the origins of each minor peak from crystal facets and the detailed transformation process of surface structures. On the other hand, only a small fraction of nanoparticles showed responses in reported PECi images, although most of them were visible in the raw SPR images, as shown in Fig.S1. This is likely due to the lack of the electrical contact between the nanoparticles and the Au substrate with the existence of the capping layers. Effectively removing the capping layers will therefore be another future aim for advancing single nanoparticle electrochemistry.

Materials and methods

Chemicals. NaOH pellets (Fisher) were dissolved in deionized water (Milli-Q, Millipore Corp.).

Sample preparation. The gold films were prepared by coating 47 nm gold on glass microscope coverslips, as described before,[22] and treated with H_2 flame before depositing AuNPs. All AuNPs samples, AuNWs (75 nm in diameter, 1 μm in length, 6.02×10^8 particles/mL), AuNRs (40 nm in diameter, 180 nm in length, 1.24×10^{10} particles/mL), and AuNCs (60 nm in size, 1.20×10^{10} particles/mL) were purchased from Nanopartz and used without future treatment. Deposition of the NPs was done by adding a few tens of μLs of the stock solution to the cell filled with 500 μL electrolytic solution and using the SPR microscope to real-time monitor the binding of the AuNPs to the gold film. In some cases, multiple attempts of deposition were needed to achieve a reasonable coverage of NPs.

Electrochemical cell. A three-electrode system (a chloridized Ag wire quasi-reference electrode, Pt coil counter electrode, and the Au chip as the working electrode) was used to induce a redox reaction on the NPs. A silicon well (cut from a flexiPERM® slide, Sarstedt) was mounted on the gold film and filled with 0.20 M NaOH solution. The exposed gold film area is approximated 0.9 cm^2. Cyclic voltammetry was applied via a potentiostat (Autolab). Unless otherwise stated, the voltammograms reported are for the first cycle with each sample. The reduction peak potential of the Au film was used as an internal standard to calibrate the potential of our CVs.

Instrumentation. The imaging setup was built on an inverted microscope (Olympus IX-81) equipped with a high numerical aperture oil-immersion objective. P-polarized light from a 670 nm SLD (SLD-260-MP, Superlum) was directed onto the gold film mounted on the objective for plasmonic excitation, and the reflected light was collected with the same objective and directed to a CCD camera for imaging.[22] The applied voltage applied between the gold electrode and reference electrode induces a redox reaction on the Au nanostructure, i.e., oxidation of the surface Au atoms, and the reduction of Au oxide, that is detected with plasmonic imaging setup, resulting in a series of images synchronized with the applied voltage.

Data extraction and processing. The raw SPR images were first converted to PECi images with imaging processing algorithms implemented with MATLAB (R2013b, MathWorks), including background subtraction (subtract first image), smoothing (on the time domain, to decrease noise) and derivative over time (subtract the current image with the previous image and divide by the time difference). The MATLAB code is provided in the supporting information. The plasmonic signal was then extracted from each frame at the tail area of each nanoparticle and plotted versus the applied potential respect to each frame for PECi CVs.

TEM images were obtained with the Philips CM200-FEG high-resolution TEM/STEM after depositing the AuNRs on copper grids.

ASSOCIATED CONTENT

Supporting Information

The Supporting Information is available free of charge on the ACS Publications website.

Supplementary data and the MATLAB code. (PDF)

AUTHOR INFORMATION

Corresponding Author

* E-mail: xshan@central.uh.edu
* E-mail: ywang184@calstatela.edu

Author Contributions

The manuscript was written through the contributions of all authors.

Notes

The authors declare no competing financial interest.
N.T.: deceased (March 2020).

ACKNOWLEDGMENT

Financial support of this work by Multidisciplinary University Research Initiative (MURI, FA9550-14-1-0003) (N. T.), new faculty start-up at University of Houston, University of Houston's High Priority Area Research Equipment Grant, High Priority Area Research Seed Grant, and Ralph E. Powe Junior Faculty Enhancement Awards (X. S.), and California State University Los Angeles (CSULA) Research, Scholarship, and Creative Activity Mini-Grant (Y.W.), and the National Science Foundation (DMR-1523588, CHE-1828334) (A.G., Y. W.) is gratefully acknowledged.

This work honors Prof. Nongjian Tao's establishment of plasmonic electrochemical microscopy and his groundbreaking works in single entity electrochemistry and the general electrochemistry field. Professor Tao's exemplary characteristics, including diligence, endless curiosity, bold and innovative ideas, grasp of both the big picture and small details, and creative vision, have greatly inspired the authors and guided their career and life for the better. Professor Tao will forever be memorialized as a mentor, a role-model, and a friend.

REFERENCES

(1) Ishida, T.; Haruta, M. Gold Catalysts: Towards Sustainable Chemistry. *Angew. Chemie - Int. Ed.* **2007**, *46* (38), 7154–7156. https://doi.org/10.1002/anie.200701622.

(2) Daniel, M.-C. C.; Astruc, D. Gold Nanoparticles: Assembly, Supramolecular Chemistry, Quantum-Size-Related Properties, and Applications toward Biology, Catalysis, and Nanotechnology. *Chem. Rev.* **2004**, *104* (1), 293–346. https://doi.org/10.1021/cr030698+.

(3) Sardar, R.; Funston, A. M.; Mulvaney, P.; Murray, R. W. Gold Nanoparticles: Past, Present, and Future. *Langmuir* **2009**, *25* (24), 13840–13851. https://doi.org/10.1021/la9019475.

(4) Prieto, A.; Hernández, J.; Herrero, E.; Feliu, J. M. The Role of Anions in Oxygen Reduction in Neutral and Basic Media on Gold Single-Crystal Electrodes. *J. Solid State Electrochem.* **2003**, *7* (9), 599–606. https://doi.org/10.1007/s10008-003-0362-3.

(5) Hamelin, A. Underpotential Deposition of Lead on Single Crystal Faces of Gold. *J. Electroanal. Chem. Interfacial Electrochem.* **1984**, *165* (1–2), 167–180. https://doi.org/10.1016/S0022-0728(84)80095-9.

(6) Adzic, R. R.; Strbac, S.; Anastasijevic, N. Electrocatalysis of Oxygen on Single Crystal Gold Electrodes. *Mater. Chem. Phys.* **1989**, *22* (3–4), 349–375. https://doi.org/10.1016/0254-0584(89)90005-9.

(7) Hamelin, A.; Sottomayor, M. J.; Silva, F.; Chang, S. C.; Weaver, M. J. Cyclic Voltammetric Characterization of Oriented Monocrystalline Gold Surfaces in Aqueous Alkaline Solution. *J. Electroanal. Chem.* **1990**, *295* (1–2), 291–300. https://doi.org/10.1016/0022-0728(90)85023-X.

(8) Hernández, J.; Solla-Gullón, J.; Herrero, E.; Aldaz, A.; Feliu, J. M. Electrochemistry of Shape-Controlled Catalysts: Oxygen Reduction Reaction on Cubic Gold Nanoparticles. *J. Phys. Chem. C* **2007**, *111* (38), 14078–14083. https://doi.org/10.1021/jp0749726.

(9) Wang, Y.; Laborda, E.; Crossley, A.; Compton, R. G. Surface Oxidation of Gold Nanoparticles Supported on a Glassy Carbon Electrode in Sulphuric Acid Medium: Contrasts with the Behaviour of "macro" Gold. *Phys. Chem. Chem. Phys.* **2013**, *15* (9), 3133–3136. https://doi.org/10.1039/c3cp44615h.

(10) Hebié, S.; Kokoh, K. B.; Servat, K.; Napporn, T. W. Shape-Dependent Electrocatalytic Activity of Free Gold Nanoparticles toward Glucose Oxidation. *Gold Bull.* **2013**, *46* (4), 311–318. https://doi.org/10.1007/s13404-013-0119-4.

(11) Hebié, S.; Napporn, T. W.; Morais, C.; Kokoh, K. B. Size-Dependent Electrocatalytic Activity of Free Gold Nanoparticles for the Glucose Oxidation Reaction. *ChemPhysChem* **2016**, *17* (10), 1454–1462. https://doi.org/10.1002/cphc.201600065.

(12) Fang, Y.; Wang, H.; Yu, H.; Liu, X.; Wang, W.; Chen, H.-Y.; Tao, N. J. Plasmonic Imaging of Electrochemical Reactions of Single Nanoparticles. *Acc. Chem. Res.* **2016**, *49* (11), 2614–2624. https://doi.org/10.1021/acs.accounts.6b00348.

(13) Wang, Y.; Shan, X.; Wang, H.; Wang, S.; Tao, N. Plasmonic Imaging of Surface Electrochemical Reactions of Single Gold Nanowires. *J. Am. Chem. Soc.* **2017**, *139* (4), 1376–1379. https://doi.org/10.1021/jacs.6b10693.

(14) Shan, X.; Díez-Pérez, I.; Wang, L.; Wiktor, P.; Gu, Y.; Zhang, L.; Wang, W.; Lu, J.; Wang, S.; Gong, Q.; Li, J.; Tao, N. Imaging the Electrocatalytic Activity of Single Nanoparticles. *Nat. Nanotechnol.* **2012**, *7* (10), 668–672. https://doi.org/10.1038/nnano.2012.134.

(15) Yu, H.; Shan, X.; Wang, S.; Chen, H.; Tao, N. Molecular Scale Origin of Surface Plasmon Resonance Biosensors. *Anal. Chem.* **2014**, *86* (18), 8992–8997. https://doi.org/10.1021/ac501363z.

(16) Zhou, S.; Ji, Z.; Shao, T. Residual Stress Evolution during Long-Term and Cyclic Aging and Annealing of Gold Films Deposited by Electron Beam Evaporation. *Vacuum* **2015**, *120* (PA), 132–138. https://doi.org/10.1016/j.vacuum.2015.07.002.

(17) Wang, Y.; Fu, W.; Hu, X. Facile Synthesis of High-Purity Single-Twinned Au Nanocrystals through Manipulation of Reaction Kinetics. *CrystEngComm* **2015**, *17* (35), 6636–6640. https://doi.org/10.1039/C5CE01000D.

(18) Carbó-Argibay, E.; Rodríguez-González, B.; Gómez-Graña, S.; Guerrero-Martínez, A.; Pastoriza-Santos, I.; Pérez-Juste, J.; Liz-Marzán, L. M. The Crystalline Structure of Gold Nanorods Revisited: Evidence for Higher-Index Lateral Facets. *Angew. Chemie - Int. Ed.* **2010**, *49* (49), 9397–9400. https://doi.org/10.1002/anie.201004910.

(19) Johnson, C. J.; Dujardin, E.; Davis, S. A.; Murphy, C. J.; Mann, S. Growth and Form of Gold Nanorods Prepared by Seed-Mediated, Surfactant-Directed Synthesis. *J. Mater. Chem.* **2002**, *12* (6), 1765–1770. https://doi.org/10.1039/b200953f.

(20) Johan, M. R.; Aznan, N. A. K.; Yee, S. T.; Ho, I. H.; Ooi, S. W.; Darman Singho, N.; Aplop, F. Synthesis and Growth Mechanism of Silver Nanowires through Different Mediated Agents (CuCl 2 and NaCl) Polyol Process. *J. Nanomater.* **2014**, *2014* (November), 1–7. https://doi.org/10.1155/2014/105454.

(21) Shan, X.; Patel, U.; Wang, S.; Iglesias, R.; Tao, N. Imaging Local Electrochemical Current via Surface Plasmon Resonance. *Science (80-.).* **2010**, *327* (5971), 1363 LP – 1366.

(22) Wang, S.; Huang, X.; Shan, X.; Foley, K. J.; Tao, N. Electrochemical Surface Plasmon Resonance: Basic Formalism and Experimental Validation. *Anal. Chem.* **2010**, *82* (3), 935–941. https://doi.org/10.1021/ac902178f.

Table of Contents (TOC)